

# T-Ray Imaging

Daniel M. Mittleman, Rune H. Jacobsen, and Martin C. Nuss, *Member, IEEE*

(*Invited Paper*)

**Abstract**—The use of terahertz pulses for imaging has opened new possibilities for scientific and industrial applications in the terahertz frequency range. In this article, we describe the technology necessary to perform terahertz “T-ray” imaging, novel imaging techniques, and commercial applications of T-ray imaging.

## I. INTRODUCTION

THE TERAHERTZ, or far-infrared, region of the electromagnetic spectrum is of critical importance in the spectroscopy of condensed matter systems, gas phase analysis, and vibronic spectroscopy of polar liquids. In the past, terahertz spectroscopy has been hindered by the low brightness of incoherent far-infrared sources and poor sensitivity of bolometric detectors. But with the advent of terahertz time-domain spectroscopy (THz-TDS) [1], [2], [3], these difficulties are overcome in a radical way. THz-TDS is based on electromagnetic transients generated opto-electronically with the help of femtosecond laser pulses. These terahertz transients are single-cycle bursts of electromagnetic radiation of typically less than 1-ps duration. Their spectral density spans the range from below 100 GHz to more than 5 THz. Furthermore, the brightness of the THz transients exceeds that of conventional thermal sources, and the gated detection is orders of magnitude more sensitive than bolometric detection.

The many advantages of the terahertz time-domain technique have resulted in rapid proliferation among researchers interested in studying properties and physical phenomena of materials in the far-infrared frequency range. On the other hand, prospects for commercial applications of this technology have been unclear so far, mostly due to the sophisticated femtosecond laser equipment needed. Within the last two years, the availability of semiconductor-diode-pumped solid-state lasers is transforming femtosecond lasers into compact, wall-plug efficient and highly practical light sources that are often not larger than an electrical power supply.

On another front, advances in the efficiency of terahertz transmitters and receivers and improved optical designs have led to the extension of terahertz time-domain techniques to real-time imaging [4], [5], [6]. This terahertz “T-ray”

technology combines imaging, real-time acquisition of terahertz waveforms and advanced signal processing techniques to obtain far-infrared images of objects and materials. In many cases, T-Ray images can also distinguish chemical compositions of the object. These features of T-ray imaging have generated interest in commercial applications in diverse areas as moisture analysis, quality control of plastic parts, packaging inspection, and trace gas analysis and monitoring. Now, with practical and cost-effective femtosecond lasers arriving on the market, vT-ray applications have the potential to become cost effective in the commercial arena.

This paper attempts an overview of the features and capabilities of T-ray imaging, and the many potential applications that this new technology has in science, industry, and manufacturing. We will also discuss novel imaging techniques such as the terahertz Hall effect and T-ray tomography, which extends T-ray technology to three-dimensional imaging.

## II. CHARACTERISTICS OF T-RAYS FOR CHEMICAL IMAGING

The potential for imaging applications using Terahertz “T-ray” pulses results from a number of characteristics. Terahertz waves penetrate most dry, nonmetallic and nonpolar objects like plastics, paper, cardboard and nonpolar organic substances. In the case of dielectrics, the absorption is governed by optical phonons and depends on the polarity and the optical phonon resonances of the material [7]. On the other hand, metals are completely opaque to T-rays, and polar liquids such as water strongly absorb in this frequency region [8], [9]. In the gas phase, most polar molecules have very sharp and strong absorption lines in this frequency range, which reflect the unique rotational or ro-vibrational spectra of the absorbing species [10], [11].

Terahertz pulses cover a broad frequency range from under 100 GHz to several terahertz. Because the terahertz time-domain technique measures these pulses in both amplitude and phase, the complex dielectric function (both amplitude and phase) can be obtained for the material under investigation when comparing input and output waveforms. A particularly useful feature of the THz-TDS technique is that this spectroscopic information manifests itself directly in the time-domain. Fig. 1 shows how different materials modify the terahertz waveforms in characteristic ways. On the top [Fig. 1(a)], the terahertz waveform after propagation through a 10-mm-thick piece of stycast is shown, together with the input pulse (dotted). The transmitted waveform shows significant “chirp,” indicative of the strong frequency-dependent refractive index of stycast. Fig. 1(b) shows the same waveform after propaga-

Manuscript received October 18, 1996; revised November 21, 1996.

D. M. Mittleman was with Bell Laboratories, Lucent Technologies, Holmdel, NJ 07733 USA. He is now with the Electrical and Computer Engineering Department, Rice University, Houston, TX 77005 USA.

R. H. Jacobsen is with the Department of Chemistry, Aarhus University, DK-8000 Aarhus C, Denmark.

M. C. Nuss is with Bell Laboratories, Lucent Technologies, Holmdel, NJ 07733 USA.

Publisher Item Identifier S 1077-260X(96)09584-6.

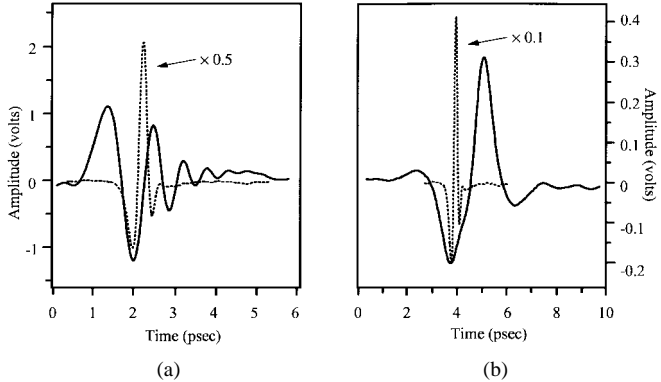


Fig. 1. Terahertz waveforms modified by passage through (a) a 10-mm block of stycast and (b) a Chinese fortune cookie. The dashed lines show the shape of the input waveform, multiplied by 0.5 in (a) and by 0.1 in (b). In (a), the transmitted pulse exhibits a strong "chirp" due to frequency-dependent index, while in (b), pulse broadening indicates preferential absorption of high frequencies.

tion through a Chinese fortune cookie. Significant broadening of the waveform is observed, indicating absorption at the high-frequency portion of the spectrum.

For T-ray imaging, the wealth of information contained in the waveforms needs to be compressed so that the relevant information can be extracted and displayed in real time, for example with the help of a digital signal processor (DSP). In the simplest case, this compression step may just be an integration of the Fourier transform of the waveform in a certain spectral range to obtain a measure of transmitted or reflected power, or a peak search to obtain the peak signal of the waveform. Because THz-TDS is a time-domain technique, another simple yet important compression step is timing extraction, for example by finding the time-delay of the waveforms after passing through materials. This is useful for example in assessing thickness variations, or in determining the position of unknown objects in reflection geometry. In more general situations, the terahertz waveforms are modified in both amplitude and phase, as shown in Fig. 1. In this case, more complex signal processing has to be performed to compress the data and extract the relevant information. For example, the strength and spectral position of sharp absorption features can be extracted using linear predictive coding (LPC) as discussed below, and broadening of waveforms can be quantitatively assessed using wavelet analysis. It is worth noting that, in many cases, the mathematical algorithms used for speech processing and recognition [12] can be modified to perform terahertz waveform processing and recognition.

### III. IMAGING SETUP

The techniques for generating, manipulating, and detecting subpicosecond terahertz pulses have been documented extensively in the literature [1]–[3]. In order to obtain images with THz-TDS, in which the entire terahertz waveform is measured at each pixel of the image, the data acquisition rate has to be increased by several orders of magnitude [4]. Also, unique aspects of the configuration of the terahertz optics used to collect and manipulate the radiation have had important implications in the imaging experiments. In addition to the

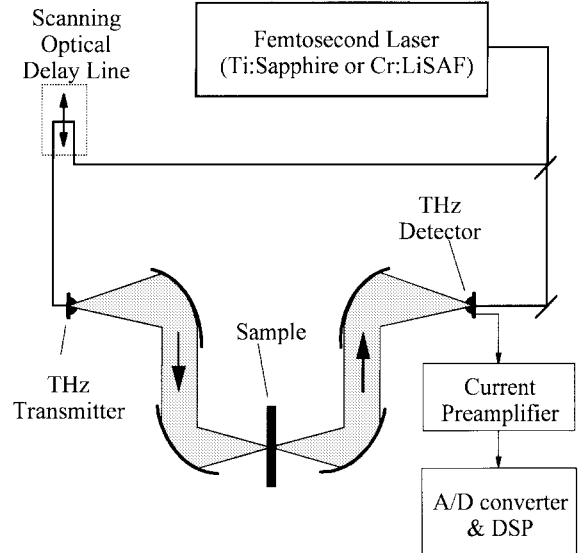


Fig. 2. Schematic of the experimental setup used for terahertz transmission imaging.

changes necessary for imaging, other advances have aided in the drive to develop THz-TDS as a viable commercial system. These have included advances in ultrafast laser technology and enhancements in terahertz generation and detection efficiency. The emphasis in this section will be those features which are new or unique to the setup used here.

Fig. 2 is a schematic diagram of a THz-TDS spectrometer, used for T-ray transmission imaging [4]. It consists of a femtosecond laser, a computer-controlled optical delay line, an optically gated terahertz transmitter, a set of off-axis paraboloidal mirrors for collimating and focusing the terahertz beam, the sample to be imaged, an optically-gated terahertz receiver, a current preamplifier, and a digital signal processor controlled by a personal computer. Although a transmission geometry is shown, terahertz images have also been generated in a reflection geometry. The apparatus used for reflection imaging is quite similar to the one depicted in Fig. 2, except for modifications to the terahertz beam path. Details of the reflection geometry will be discussed below (see Fig. 9).

#### A. The Ultrafast Laser Source

Although an argon-laser pumped femtosecond Ti:Sapphire laser is used for most of the experiments presented in this article, we cannot overlook recent advances in solid-state mode-locking that are revolutionizing the field of ultrafast optics and applications. New laser sources, such as the diode-pumped Cr:LiSAF, are capable of producing trains of pulses with duration less than 100 fs and with average powers greater than 100 mW [13]–[16]. These sources are compact, reliable, and less expensive to operate and maintain than the more conventional Ti:Sapphire systems. Active research in the mode-locking of doped fiber lasers promises to advance femtosecond technology even further, to the point where the ultrafast laser source will no longer be the largest and most expensive component of a terahertz spectrometer. This migration will require development of terahertz transmitters

and receivers capable of operating at  $1.5 \mu\text{m}$ , where most fiber lasers operate. These advances in femtosecond laser technology are a key enabler of a portable THz-TDS spectrometer.

### B. THz Optoelectronic Switches

While the terahertz transmitter and receiver designs were identical in early THz-TDS work, more efficient structures have been devised in both cases. Fig. 3(a) shows the design of a high-efficiency transmitter structure [17]. The antenna consists of two  $10\text{-}\mu\text{m}$ -wide metal lines deposited on semi-insulating GaAs, with a separation of  $100\text{ }\mu\text{m}$ . Two metal tabs extend out from these lines toward each other; these tabs may terminate in either flat or triangular ends. The gap between the two tabs is roughly  $50\text{ }\mu\text{m}$ . A voltage of  $\sim 75\text{ V}$  is applied across the two lines, creating a strong depletion field near the anode. Focusing about  $50\text{ mW}$  of the femtosecond beam near the corners or points of the anode structure greatly enhances this depletion field [17], [18]. This can lead to an enhancement in the strength of the emitted terahertz field, by roughly a factor of 3–5 [17]. Fig. 3(b) shows the enhancement of the emitted terahertz field, as the laser focus is moved into the vicinity of the point of the anode.

The most commonly used terahertz receiver has been a simple dipole antenna, roughly  $\sim 50\text{ }\mu\text{m}$  in length, deposited on radiation-damaged silicon-on-sapphire (rd-SOS) [1]. This material has been demonstrated to provide an excellent high frequency response, producing terahertz pulses shorter than  $400\text{ fs}$  [1], [19]. Another material with fast response time and high mobility is low-temperature grown GaAs (LT-GaAs) [20]. An advantage of LT-GaAs is the higher optical damage threshold, which permits the use of over  $50\text{ mW}$  of optical power in the gating beam. Since the measured terahertz signal increases with the power in the gating beam, these materials can provide considerably higher signal levels, compared to rd-SOS detectors.

### C. Terahertz Beam Optics

A key ingredient to a high-performance T-ray imaging system is an optical system that 1) allows one to focus the terahertz waves to a diffraction-limited focal point at the object and 2) has the highest possible throughput. Unlike in optical systems designed for visible light, the wavelength of the terahertz electromagnetic signals is not negligible compared to the size of the optical elements used, and diffraction effects can dominate ray-propagation. This can be a significant complication in the design of optical systems for the terahertz frequency region. Additionally, because of the large spectral bandwidth, the optical system needs to be chromatic and exhibit a flat phase response over the frequency range of the pulse.

A critical component that enables these features of the terahertz beam system are the substrate lenses, which are attached to the backs of the transmitter and receiver chips. The substrate lenses improve the coupling of the light into and out of the photoconducting antennas, and do so without degrading optical beam properties. In previous terahertz beam systems, these requirements were difficult to meet [2], [21],

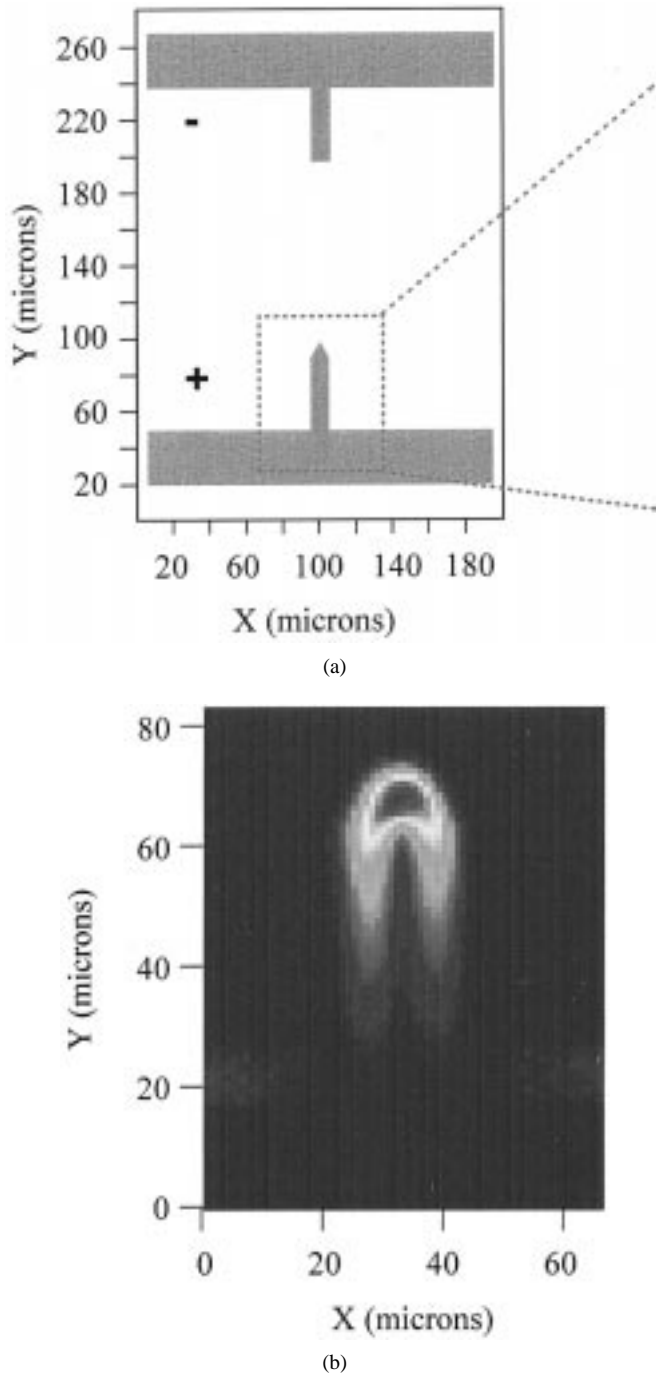


Fig. 3. (a) Design of a high-efficiency terahertz transmitter, showing the shape of the structured metal electrodes, (b) False color image depicting the strength of the emitted field as a function of the position of the laser focus. The terahertz field is strongly enhanced in the vicinity of the field singularity (after [17]).

because the transceivers were located at the focal point of the substrate lens. This has two detrimental effects: first, only the portion of the light close to the optical axis of the lens is coupled out of the lens into air—light emitted at larger angles is lost due to internal reflection at the lens-air interface [21]. Second, the beam diameter at the exit pupil of the lens is only a few millimeters for the typically 10-mm diameter substrate lenses; this leads to serious diffraction effects at the exit pupil, which in turn leads to difficulties in collimating and focusing

the terahertz beam. In fact, a collimated beam with frequency-independent beam diameter and without wavefront curvature cannot be obtained using this substrate lens design [22].

These problems can be avoided by modifying the substrate lens design. Use of hemispherical substrate lenses, for which the antenna is located at the center of radius of the lens, completely eliminates all diffraction and total internal reflection effects as no refraction occurs at the lens-air interface. However, the cone angle of the terahertz emission can be quite large, so that optics with very large numerical aperture is required to subsequently collimate the beam. An excellent compromise is the aplanatic hyperhemispherical substrate lens. In this design, the dipole is located at a distance  $h$  from the tip of the lens given by

$$h = R \left( 1 + \frac{1}{n} \right)$$

where  $R$  is the radius of the lens and  $n$  is its refractive index. Like the hemispherical lens, this lens design has no spherical aberration or coma and, when using silicon as a substrate lens material, no chromatic aberration throughout the terahertz range [23]. Using this lens design, we obtain collimated terahertz beams with essentially no frequency-dependent beam diameter, and achieve diffraction-limited focusing to a  $300\text{-}\mu\text{m}$  focal spot at a center frequency of 1 THz.

#### D. Signal Acquisition

The traditional method for acquiring terahertz waveforms has relied on a photoconductive sampling technique, in which the delay of one of the gating pulses is swept relative to that of the other, and the average photocurrent generated in the receiver is measured as a function of the delay. The resulting signal is the convolution of the terahertz waveform with the temporal shape of the photoconductive sampling gate. Most of the time, the signal is acquired with a lock-in amplifier, and one of the gating beams (or the terahertz beam) is modulated with a chopper wheel. Since this requires a lock-in time constant in the range of tens to hundreds of milliseconds, the sweep time of the delay is quite slow, on the order of hundreds of milliseconds per data point. At this rate, it takes several minutes to acquire a single 1024-point terahertz waveform.

In order to obtain images, where the entire waveform is measured and analyzed at each pixel, this acquisition time must be reduced dramatically. To accomplish this, the slow stepper motor that provides the optical delay is replaced with a scanning optical delay line (ODL). The ODL (Clark-MXR) used in our experiments, a retro-reflecting mirror mounted on a galvanometric shaker, provides roughly 3 cm of optical path delay on each sweep, and can sweep at up to 100 Hz. With this device, the lock-in amplifier and the chopper wheel are no longer necessary. Dispensing with the noise filtering provided by the lock-in detection does degrade the signal-to-noise somewhat, but allows for much faster acquisition times. As a result, the noise is larger by a factor of between 20 and 100 compared to the slow scan using lock-in techniques. But this is more than compensated by the various transmitter, receiver, and optics improvements described above. Fig. 4

shows a waveform measured with a single sweep of the ODL; in Fig. 4(b), the amplitude spectrum of this waveform is shown on a semi-log scale. Each of the 1024 points in this waveform was acquired in roughly 25 microseconds, and the result has a signal-to-noise of approximately 1000, as seen by the noise baseline above  $\sim 3$  THz. Much of the residual noise in this data arises from power fluctuations in the femtosecond laser, which in turn can be traced to plasma instabilities in the argon-ion pump laser [24]. By moving to an all-solid-state laser system like a Cr:LiSAF laser, this noise source can be effectively eliminated. Thus, it should be possible to measure up to 100-THz waveforms in a second, with a signal-to-noise in each that approaches the one that has been previously reported using slow scanning methods.

#### IV. T-RAY IMAGING

The above descriptions of various aspects of the THz-TDS apparatus, when taken together, represent significant improvements in the portability, reliability, and cost of the system, as well as the overall quality of the terahertz signals. For these reasons, it is now feasible to consider “real-world” applications of terahertz imaging. As described below, a number of applications, in an extremely diverse array of fields, may benefit significantly. For some problems, THz-TDS may be the only technology available to address the issue, while in other cases, it may be that alternative technologies are simply too expensive, inefficient, or impractical. Although the following discussion explores a number of potential uses of terahertz imaging and touches on examples in each of these areas, it is by no means an exhaustive list.

As mentioned in Section I, the industries and applications areas discussed here are quite wide ranging; they are dictated by the characteristics of the terahertz radiation. Many of the applications under consideration rely on either the extreme sensitivity to water or the ability to propagate through common packaging materials, or both. All of these abilities can be combined with the imaging capabilities. In many applications, a reflection geometry will be of substantial advantage, or may even be required. Although much of the work reported so far relies on transmission imaging, it should be emphasized that imaging in reflection is quite feasible, and even affords some additional advantages, as discussed below.

Also important is the ability to detect and identify most polar molecules in the gas phase. This application relies on the broad bandwidth of the radiation, and the fact that, as in the mid-infrared, many molecules have characteristic “fingerprint” absorption spectra in the terahertz region. This has been exploited in the development of an automated real-time gas monitoring system [25]. This system may be a powerful complement to the established gas monitoring devices which are based on FTIR technology, and which rely on the mid-infrared “fingerprint” absorption spectra of such gases as CO, CO<sub>2</sub> and methane. These gases are not highly polar, and therefore do not show significant absorption in the terahertz region. Conversely, polar molecules such as ammonia and HCl absorb quite strongly, with characteristic features within the

bandwidth of the terahertz pulse, but are more difficult to detect using other optical means.

In the following paragraphs, we will discuss a number of applications of T-ray imaging to illustrate these classes of applications.

### A. Terahertz Imaging of Moisture

The simplest type of image one can generate in a transmission imaging setup is one in which the transmitted power determines the nature of the image. In our system, this is accomplished using the digital signal processor, which performs a fast Fourier transform of the waveform in real time, and integrates the magnitude of the resulting power spectrum over a certain spectral range. Because of the diffraction-limited focus at the sample, integration over only the high-frequency part of the terahertz spectrum will improve the spatial resolution; conversely, integrating exclusively over the low-frequency portion minimizes the effects of scattering losses, which rise as the fourth power of the frequency [26].

A good example of this is shown in Fig. 5, which shows a terahertz transmission image of a leaf from a common houseplant. The color scale is determined by the amplitude of the transmitted terahertz power, which in turn is related to the amount of moisture present at each point on the leaf. (The dashed box across the figure refers to the measurements of Fig. 6, discussed below.) This image illustrates the extreme sensitivity of this technique to water content. In this frequency range, water absorbs quite strongly. Recently, Keiding and co-workers [8] measured the absorption coefficient of liquid water, using THz-TDS in a reflection geometry. Their value of  $\alpha \sim 230 \text{ cm}^{-1}$  at  $\nu \sim 1 \text{ THz}$  has been confirmed by transmission measurements, and is in reasonable agreement with molecular dynamics simulations [9]. This value has direct implications for the ultimate sensitivity of terahertz imaging to changes in water content. With a signal-to-noise of 100:1 in the measured electric field, the minimum detectable water concentration is given by  $n \cdot x \sim 10^{16} \text{ cm}^{-2}$ , where  $n$  is the density of water molecules and  $x$  is the length of the path traversed by the terahertz beam in the material. In a material with a thickness of 1 mm, this implies a detection limit of less than  $10^{-5}$  of liquid density.

This extreme sensitivity to water content can be exploited in measurements such as those illustrated by Fig. 5. Indeed, this is of great interest as a method of measuring the water content of leaves on *living* plants. Currently, there is no accepted, nondestructive procedure for measuring the leaf water status of a transpiring plant. Research in the field of plant water relations has been limited to point-in-time observations that provide average values across the tissue being studied [27]. Multiple spatial and repeated temporal observations have been required to account for the dynamic movement of water through the plant and for spatial variation in water status in individual leaves. Using terahertz imaging, it is possible to account for inhomogeneities in the sample by performing a spatially resolved measurement. Because these measurements are inherently nondestructive, repeated measurements may be made on the same tissue, thereby providing for the study of

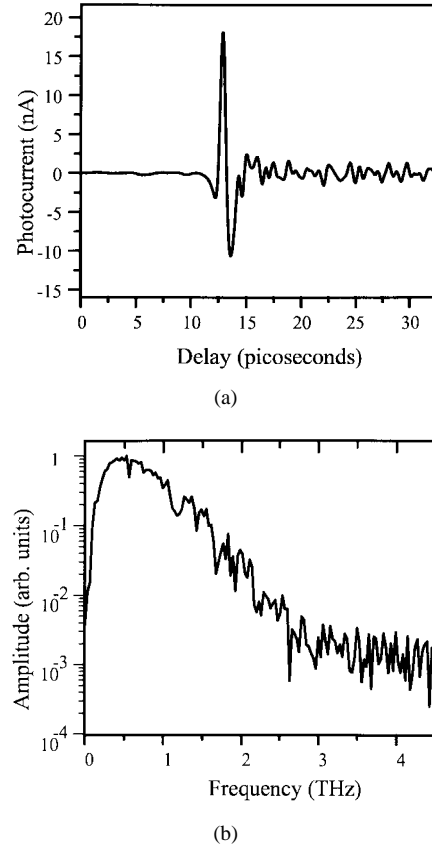


Fig. 4. (a) Terahertz waveform measured in a single scan of the ODL; (b) Magnitude of the Fourier transform of the waveform in (a), on a semi-log scale. The noise baseline is roughly 1000 times lower than the peak signal. The oscillations which follow the main pulse, and which appear as modulations on the spectrum, are a result of water vapor in the beam path, and do not significantly affect the signal-to-noise estimates in the text.

water flow dynamics. A demonstration of this application is shown in Fig. 6, in which the amplitude of the transmitted terahertz radiation is shown as a function of horizontal position across a leaf, at various delay times after the plant was watered. The approximate location on the leaf of these line scans is shown by the dashed box in Fig. 5. In Fig. 6, the variations observed as a function of position on the leaf, which are repeated at each delay time, reflect the different transmission coefficients through different parts of the sample. These result primarily from the stem structure; as seen in Fig. 5, the region of the line scans intersects the primary or central stem, as well as a number of subsidiary stems on either side. As a function of time after watering, the transmission decreases by several percent, indicating that water is absorbed into the leaf on a time scale of hours. Experiments such as this can be used to further understand the early warning signs of plant water stress, and may be valuable aids in irrigation management for a wide range of crops.

### B. Terahertz Imaging for Quality Control

Spatially resolved measurements of the terahertz transmission coefficient may also be used in package inspection or quality control applications. Evidently, since many packaging materials such as plastic and cardboard are transparent to

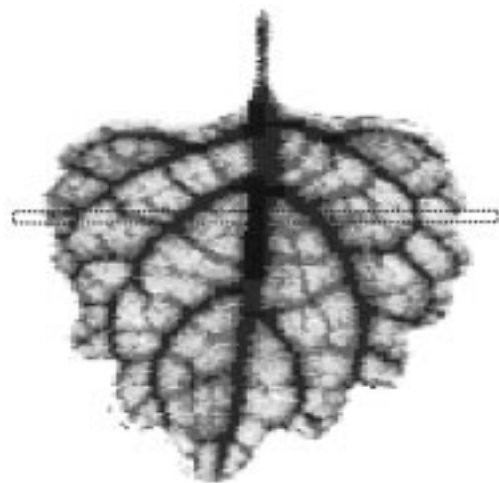


Fig. 5. Terahertz image of a leaf from a common houseplant, Coleus. The false color scale is correlated with water content, with darker green indicating more water. The dashed box indicates the approximate position of the line scans of Fig. 6, as described in the text.

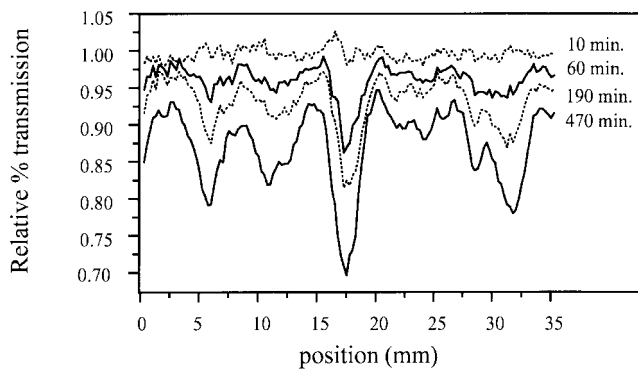


Fig. 6. Terahertz line scans along a line that transects the center of the leaf, as shown by the dashed box in Fig. 5. The modulation in each line scan results from the stem structure of the leaf. Each scan is labeled according to the time (in minutes) after the plant was watered. Decreasing terahertz transmission results from water intake into the leaf tissue.

terahertz radiation, it is quite simple to image through these materials and detect the contents. In many industries, X-ray imaging is currently used for such tasks. T-ray imaging may be a desirable alternative simply because of the health and safety issues involved with ionizing radiation. Because of the low energies of the photons involved and the extremely low intensities generated, T-rays present virtually no safety concerns, particularly if the femtosecond laser pulses are delivered to the terahertz switches via optical fiber. The extreme sensitivity to water content proves important in these types of applications as well. Although numerous methods exist for measuring the water content of moisture-sensitive products, essentially no method exists if the measurement must be performed through a cardboard or thin plastic package. Preliminary tests on samples such as shrink-wrapped food products indicate that the amplitude of the reflected terahertz pulse is a good measure of the moisture content of the surface layer of the product.

Fig. 7 illustrates another use of terahertz imaging as a quality control monitor. This figure shows the terahertz image of a manufactured part, representative of innumerable mold-

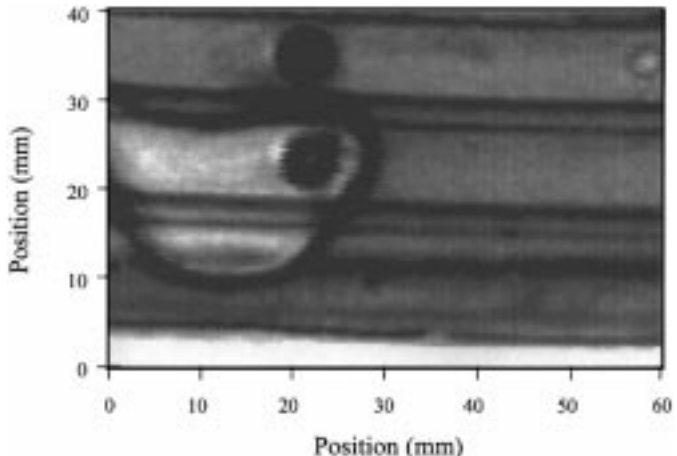


Fig. 7. Terahertz image of a molded composite plastic piece, as described in the text. The image clearly shows the presence of a roughly circular  $\sim 2\text{-cm}$  void in the internal foam-filled region.

fabricated plastic piece-parts. This part consists of two parallel black plastic sheets, with a rubberized foam padding between them. In the manufacturing process, the foam is sprayed between the plastic sheets, holding them together when it dries. However, occasionally bubbles or voids develop in the foam, sometimes as large as an inch in diameter or more. Detection of these voids is a significant quality control issue, and no simple method currently exists. X-ray transmission does not provide a high contrast between the plastic-rubber foam and the air; in addition, health and safety issues preclude the use of X-ray diagnostics here. Ultrasound analysis is effective only with the use of an index-matching fluid, while other probing techniques such as magnetic resonance imaging are too expensive and cumbersome. Probing the parts with microwaves would work quite nicely, except that it would be difficult to detect voids significantly smaller than the wavelength of the radiation used. Since, in this case, it is desirable to detect voids smaller than one centimeter in diameter, this effectively eliminates conventional microwave analysis from consideration.

The terahertz imaging technique exploits the fact that the rubber foam filling has many tiny air pockets, which act as good scattering sites for radiation in the 0.5-mm wavelength range. Of course, the solid plastic surfaces on the front and rear of the sample are fairly transparent to the terahertz radiation. As shown in Fig. 7, the terahertz image clearly locates the void, simply by observing an increase in the transmission through the sample wherever a smaller length of foam is traversed. Terahertz imaging is extremely sensitive to small voids or other morphological variations which may occur inside solid plastic or plastic composite parts. It may seem somewhat fortuitous that the foam rubber in this particular example consists of scattering sites ideally suited for the wavelength range spanned by the terahertz pulses. It should be emphasized that one could detect voids of this sort without relying on such a coincidence by observing the *transit time* of the terahertz pulse through the material, rather than the transmitted *amplitude*. The combination of the amplitude and phase information measured in THz-TDS make for a very powerful tool for quality control measurements.

### C. T-Ray Tomography

Because the technique of THz-TDS relies on a coherent detection scheme, in which the electric field of the terahertz pulse is measured explicitly, the detected waveforms typically contain far more information than simply the power transmission coefficient of the sample under study. Changes in the phase of the measured waveform also can frequently be correlated with important properties of the sample. As a crude measure of phase changes, one may simply monitor the change in the arrival time of the peak (or first zero crossing) of the terahertz waveform. Changes in this arrival time as a function of position on the sample indicate changes in the optical path length of the terahertz beam, relative to the femtosecond beam. This may result from either changes in the thickness of the sample as it is scanned transversely across the terahertz beam, or changes in the refractive index, or both. The change in arrival time  $\Delta t$  is given by  $\Delta t = \frac{1}{c} \int n(z)dz$ , where  $n(z)$  is the refractive index seen by the terahertz beam along its optical path, and where the integral is along the path. An illustration of this technique is shown in Fig. 8, in which a small gas flame has been imaged in transmission. In this experiment, the ionized molecules which make up the flame may have a significant absorption at certain frequencies within the spectrum of the pulse [28], but the gas density is so low that this effect cannot be observed. However, the flame heats the air locally, which changes the refractive index along the terahertz optical path  $n(z)$ . A crude estimate of the magnitude of this effect would assume that the refractivity of air varies inversely with temperature. If the flame has a thickness of roughly 5 mm, this would lead to a shift in the transit time of the terahertz pulse by  $\sim 3$  fs for a flame of 1000 °C [29]. Each contour in Fig. 8 represents a shift of 5 fs in transit time.

One can imagine performing time-of-flight measurements in a reflection geometry similar to those described in the transmission experiment above [30]. Fig. 9 shows the modified beam path for reflection geometry, in which the terahertz beam focuses at the sample, and is reflected at near normal incidence. This presents a situation which is quite analogous to optical coherence tomography (OCT), a technique which has achieved considerable success in recent years in such fields as ophthalmology and developmental biology. In an OCT device, a short coherence length light source is split into two beams; one is reflected off of the sample and the other off of a reference. The two are then correlated to provide information about the reflectivity of the sample [31], [32]. Distance measurements are possible because a correlation signal is only measured when the path length of the reference arm is equal to that of the sample arm, within the coherence length of the light source. As a result, the ultimate spatial resolution achieved in depth (i.e., the propagation direction of the reflected beam) is limited by the coherence length of the source. As illustrated above, the terahertz tomographic measurement is not limited in the same way. The coherence length of a terahertz pulse is determined by the pulse duration, which is on the order of several hundred femtoseconds. However, the measurement of the flame presented above is sensitive to temporal shifts as small as 5 fs. This sensitivity stems from the phase-sensitive nature of

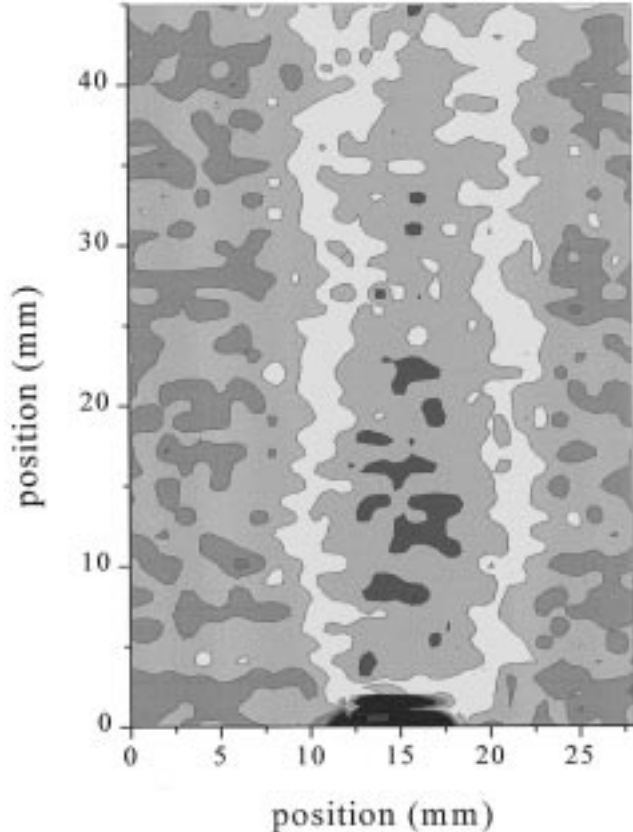


Fig. 8. Terahertz image of a small gas flame. This image is formed by measuring the transit time of the terahertz pulse through the flame, and encoding shifts in this time in false color. Each contour corresponds to a 5-fs shift in the time delay, which results from local heating of the air, as described in the text. The gas nozzle is visible in black at the bottom center of the figure.

the measurement, and from the fact that each terahertz pulse is a single cycle of the electromagnetic field. It is possible to measure the zero-crossing of an electric field much more accurately than the peak of an intensity autocorrelation. Using this simple idea, it is possible to measure changes in either refractive index or thickness with extremely high accuracy. For example, one can detect, in transmission, a single sheet of paper added to a stack; in reflection, it is possible to achieve a depth resolution of approximately 1  $\mu\text{m}$ . The limitation in this measurement is simply the accuracy with which the optical scanning delay line repeats its position on each scan.

The idea of T-ray tomography is illustrated in Fig. 10, which is a T-ray image, taken in reflection, of a ball-point pen. A pen is an ideal sample for demonstration of this technique, because it consists of a number of smooth, well-separated dielectric interfaces. The vertical axis is parallel to the long (cylinder) axis of the pen, while the horizontal axis of the figure corresponds to depth inside the pen. Fig. 11 shows the input and output waveforms. The output waveform Fig. 11(b) consists of a series of reflected replicas of the input waveform. Each reflection originates from one of the eight dielectric interfaces, either from air to plastic or from plastic to air, formed by the two concentric plastic cylinders which form the pen. These eight surfaces are observed, tomographically, in Fig. 10. This technique is particularly interesting because,

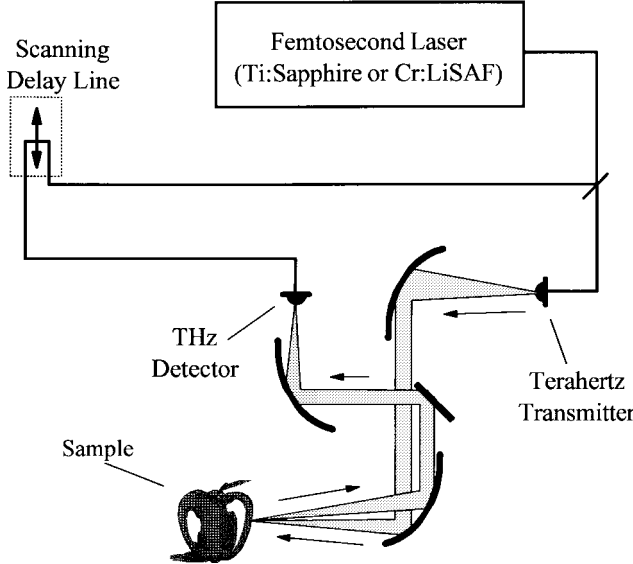


Fig. 9. Schematic of the setup used for terahertz reflection images. The terahertz beam is incident on the sample at near normal incidence, and is focused onto it with a confocal parameter of  $\sim 1$  cm.

in a case such as this where the reflecting surfaces are reasonably well separated in space, each reflected pulse may be isolated in time, and analyzed for spectral information. In other words, each successive reflection contains chemical or spectral information about the additional layers traversed. This idea is illustrated in a rudimentary way in this example; from simply noticing the alternating polarity of the eight reflected pulses Fig. 11(b), one can immediately determine the sign of the refractive index change at each interface. One can also note in Fig. 10 that the rear plastic walls in the upper portion of the figure are not visible; this results from the shadow cast by the ink, an excellent absorber of terahertz radiation, inside the inner cylinder.

#### D. Terahertz Tomography for Burn Diagnostics

A technique such as terahertz tomography may be of great interest in a wide range of applications. One example, which presents somewhat more of a challenge in interpretation than the example illustrated above, is in the area of burn diagnostics. While the strong water absorption precludes the use of terahertz radiation in most biomedical research areas, those which are particularly concerned with surface (e.g., dermatological, corneal, etc.) issues may find the unique properties of these submillimeter waves to be of interest. In particular, it may be possible to obtain quantitative and highly sensitive measurements of burn depth using terahertz tomography.

The noncontact measurement of burn depths and severities using photonics is a topic of considerable interest [33], [34]. In this field, it is not uncommon to use uncooked chicken breasts as a model for tissue, in order to gain some rudimentary understanding of the tissue–radiation interaction. A chicken breast is burned in several spots with a soldering iron; the severity of the tissue damage is varied simply by controlling the duration of the burn. The entire sample is then covered

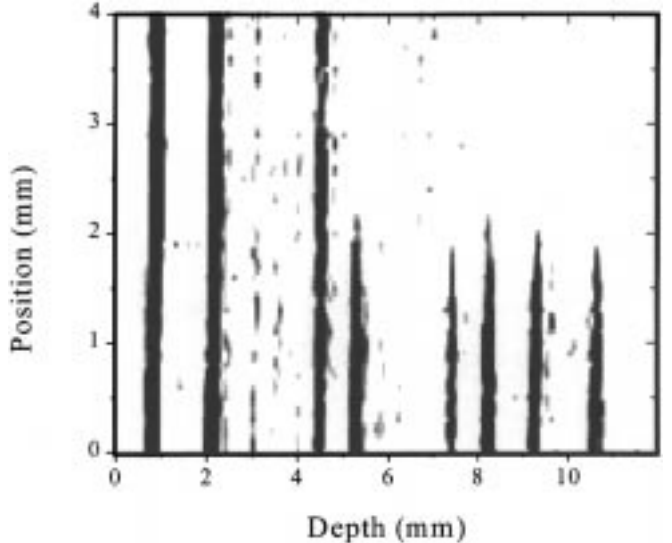


Fig. 10. Terahertz tomographic image of a bic pen. The vertical axis of the figure is parallel to the long (cylinder) axis of the pen, while the horizontal axis of the figure corresponds to depth into the pen. The terahertz pulse is incident from the left. The eight dark lines correspond to the eight dielectric interfaces (either from plastic-to-air or air-to-plastic) encountered by the pulse as it propagates through the pen. The upper right portion of the image is obscured, because these surfaces were shadowed by ink inside the inner plastic cylinder.

with a thin ( $\sim 1$  mm) slab of polystyrene, which serves two purposes. First, it keeps the sample flat and stationary during the measurement. Second, the terahertz pulse reflected off of the outer surface of the polystyrene (i.e., the air-plastic interface) serves as a reference pulse, both in amplitude and in delay time, for the subsequent reflections from the tissue underneath. Fig. 12 shows the reflected pulse trains measured at four different points on the sample. The upper pulse train [Fig. 12(a)] corresponds to a measurement of healthy tissue. Here, it is observed that a second pulse, reflected from the interface between the polystyrene and the healthy tissue, follows the reference pulse and closely resembles it. The remaining three pulse trains correspond to measurements of areas with increasing burn severities. Evidently, the pulse reflected from the plastic-tissue interface no longer resembles the reference pulse. Indeed, it appears that, in the case of the most severely damaged tissue, there may be a third reflection a few picoseconds after the second. This may arise from a reflection at a (buried) interface between tissue with no water and tissue with some substantial water content. Clearly, these reflected pulses contain a great deal of information about the dielectric properties of the damaged tissue. Disentangling the details of this information and correlating it with physiological variables will require a good deal of effort, and many more experiments. Nonetheless, this data demonstrates a powerful new technique and a potentially valuable diagnostic tool in biomedical optics.

#### E. The Terahertz Hall Effect

An example of an application of terahertz imaging in which both the amplitude and phase of the transmitted wave are used to form an image, is found in the field of semiconductor wafer characterization [35]. A powerful tool in the characterization

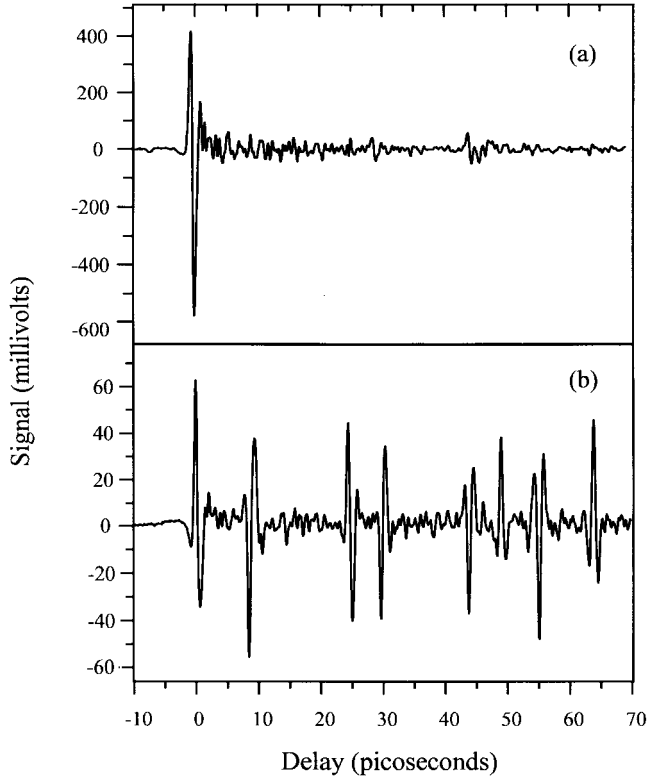


Fig. 11. Terahertz waveforms (a) incident on, and (b) reflected from the bic pen shown in. The small oscillations which follow the main pulse in (a) are a result of residual water vapor in the beam path, and do not significantly affect the measurement. A reflected pulse from each of the eight dielectric interfaces can be observed in (b). The polarity of the reflected pulse immediately allows one to determine the sign of the change in refractive index at each interface.

of doped wafers is the Hall effect. This effect, in which an applied voltage induces a transverse voltage in the presence of a large dc magnetic field, is commonly used to measure material properties of any conducting sample. Indeed, it is the method of choice for measurements of dc properties in thin doped epitaxial layers of semiconductors. A measurement of the Hall parameters is equivalent to measuring the full complex conductivity tensor of the sample. From this measurement, both the mean carrier density and the carrier mobility can be determined. However, it is necessary to contact the sample at four points. The results must be considered as a spatial average over the region contained within the four point contacts. As always in such experiments, contact resistance must be carefully controlled, and can easily lead to spurious results.

It is possible to extract the same information using the terahertz field as the applied electric field in the Hall experiment. A schematic of the experiment is shown in Fig. 13. The samples consist of a 1- $\mu\text{m}$ -thick layer of either n- or p-doped GaAs, epitaxially grown on a  $\sim 0.5$  mm undoped GaAs substrate. In the presence of a magnetic field pointing parallel to the beam propagation direction ( $\hat{z}$ ), the applied terahertz field (along  $\hat{x}$ ) induces a current (also along  $\hat{x}$ ) which in turn induces a Hall field, oriented in the transverse direction (along  $\hat{y}$ ). This Hall field radiates a terahertz field which is coherent relative to the input terahertz beam, but which is polarized orthogonally to it. A measurement of the amplitude and phase of this radiated

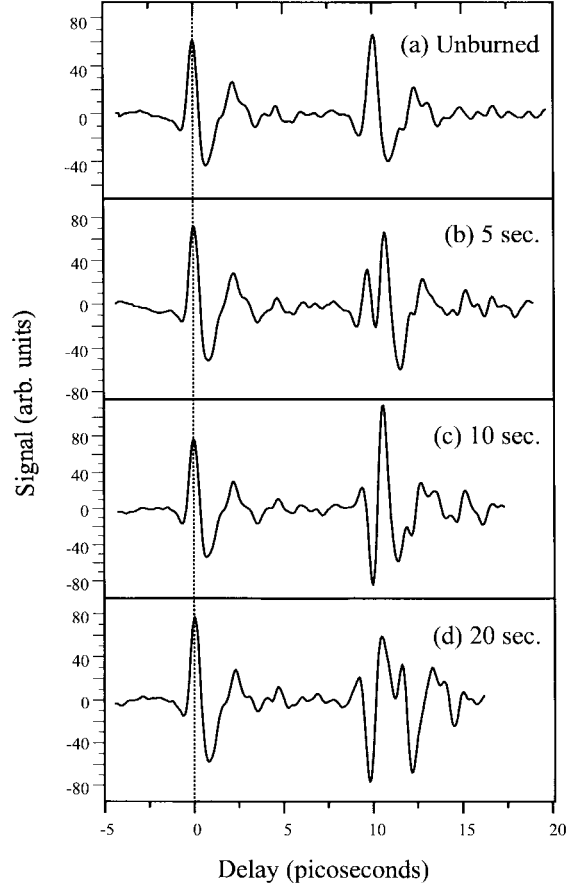


Fig. 12. Terahertz waveforms reflected from various spots on a piece of raw chicken breast: (a) reflection from healthy tissue, (b) tissue which had been burned for 5 s, (c) 10 s, and (d) 20 s. The initial pulse is reflected from a thin plastic overlayer, and can be used as a reference for both delay time and amplitude, as described in the text. The distortions of the reflections from the burned areas could be used to extract quantitative information about the dielectric properties of the damaged tissue.

beam can be used to determine the conductivity tensor of the sample. In practice, the incident field is polarized at  $45^\circ$  to the vertical axis, and both the vertical ( $\hat{y}$ ) and horizontal ( $\hat{x}$ ) fields are measured simultaneously, with two orthogonally oriented detectors. This phenomenon is related to the early work of Chambers and Jones [36], although in somewhat different physical limits. More recently, a technique using millimeter-wave near-field imaging with similar capabilities has been reported [37].

In the absence of a magnetic field (or in the absence of a sample), the polarizing beamsplitter can be adjusted so that these two measured fields are approximately equal. Then, when the magnetic field is applied to the sample, the two waveforms should be quite different, as the Hall effect transfers energy between the two orthogonal waves. Fig. 14 shows the spectra of  $\hat{x}$ - and  $\hat{y}$ -polarized terahertz waveforms without a magnetic field, with a magnetic field of  $\sim 1.3$  T, and with the same magnetic field in the opposite direction. This serves as a clear demonstration of the terahertz Hall effect. These two terahertz waveforms can be used to calculate both the carrier density and carrier mobility directly, using the semiclassical Drude theory.

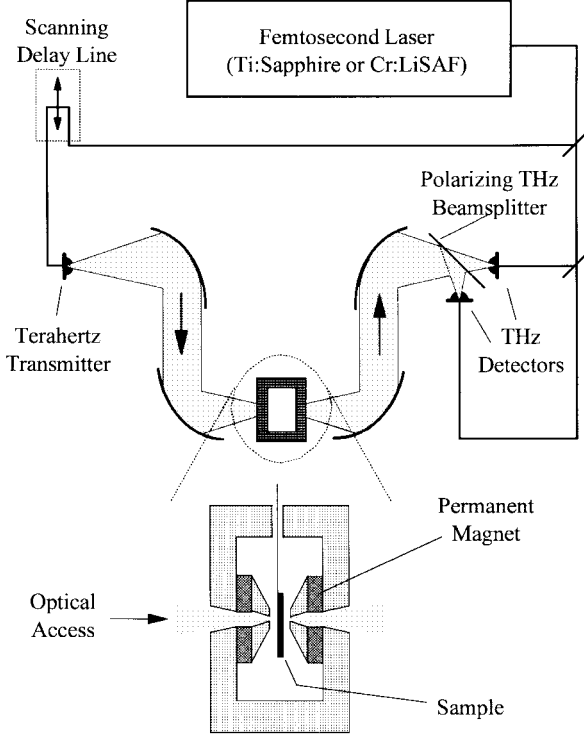


Fig. 13. Schematic of the setup used for terahertz Hall effect measurements, showing permanent 1.3-T magnet, free-standing wire grid polarizing beam splitter, and two receivers operating in parallel for simultaneous detection of two orthogonal polarizations.

The Drude model describes fairly accurately the behavior of the carriers in moderately doped semiconductors [38], [39]. Within this formalism, the magnetoconductivity tensor has two independent values, the diagonal ( $\sigma_{xx}$ ) and off-diagonal ( $\sigma_{xy}$ ) element. These are related to fundamental parameters by the relations

$$\sigma_{xx} = \sigma_0 \cdot \left( \frac{1 - i\omega\tau}{(1 - i\omega\tau)^2 + (\omega_c\tau)^2} \right) \quad (1)$$

$$\sigma_{xx} = \sigma_0 \cdot \left( \frac{\omega_c\tau}{(1 - i\omega\tau)^2 + (\omega_c\tau)^2} \right) \quad (2)$$

where  $\omega_c$  is the cyclotron frequency, proportional to the magnetic field,  $\sigma_0$  is the dc conductivity,  $\sigma_0 = N e \mu$ , and  $\tau$  is the Drude scattering time. Here,  $N$  is the carrier density, and  $\mu$  is the mobility, given by  $\mu = e\tau/m^*$ . Of course, the off-diagonal element vanishes as  $B \rightarrow 0$ , since the magnetic field provides the transverse coupling in the Hall effect. In this experiment, the doped layer is much thinner than one wavelength, so for the purposes of the propagation this is a surface charge layer. Thus, the experiment measures the *sheet* conductivity, and the carrier density which appears in  $\sigma_0$  is the *sheet* carrier density [40]. The quantities in (1) and (2) can be related to the input terahertz fields, measured with no sample in the beam, by taking into account the reflection losses at both ends of the sample and the (small) absorption and dispersion effects in the thick undoped substrate, and by using the tabulated values of  $n(\omega)$  and  $\alpha(\omega)$  for intrinsic GaAs [7]. By so doing, the two terahertz fields can be used to independently determine absolute numerical values

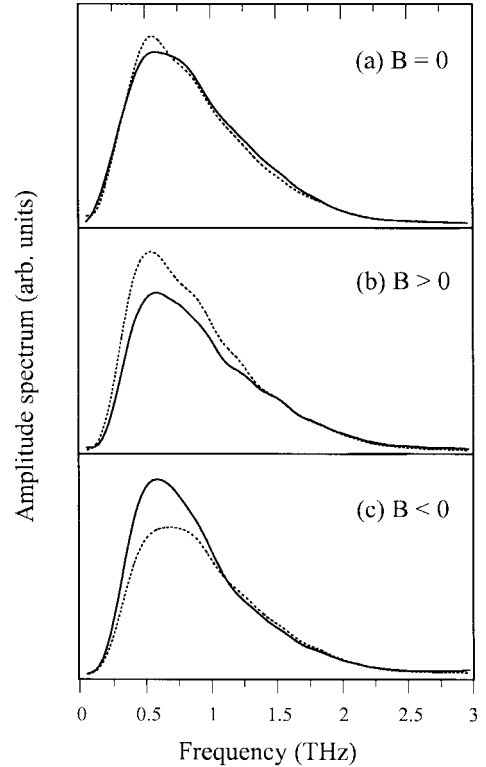


Fig. 14. Terahertz waveforms transmitted through a n-doped sample, of the type described in the text. The nominal doping density for this sample was  $1.9 \times 10^{17} \text{ cm}^{-3}$ . The input terahertz field is polarized at  $45^\circ$ ; the two curves correspond to the horizontal (solid) and vertical (dashed) components. In (a), no magnetic field is applied, and the two measured components are approximately equal, while in (b) a field of  $\sim 1.3$  Tesla is applied to the sample in a direction parallel to the terahertz beam propagation. In (c), the same field is applied in the opposite direction. The transfer of energy between the orthogonal components of the field is evidence of the terahertz Hall effect.

for the carrier density  $N$  and the mobility  $\mu$ . This entire calculation can be performed rapidly enough that it can be incorporated into the imaging software, thus permitting real-time imaging of these two important material parameters. Inhomogeneities in both  $N$  and  $\mu$  can be imaged with a spatial resolution of  $\sim 250 \mu\text{m}$ , roughly an order of magnitude better than the best four-point probe measurements. Fig. 15 shows two such images, one for each of  $N$  and  $\mu$ , generated with an *n*-GaAs sample with a nominal doping density of  $1.9 \times 10^{17} \text{ cm}^{-3}$ , as determined by growth conditions. With these techniques, *in situ* noncontact characterization of the uniformity of semiconductor wafers should be possible.

#### F. Time-Domain Waveform Analysis

The implementation of fast scanning and real-time data acquisition in THz-TDS has focused attention on new ways of analyzing and processing waveforms. In particular, fast and efficient algorithms are important for chemical recognition systems [25], where spectroscopic information is processed in real-time with the aim of determining the chemical compositions of an object. For real-time recognition systems, such as in speech recognition [12], a common strategy is to perform a signal compression, i.e., to parameterize the characteristic response, and to use these parameters in a subsequent pattern

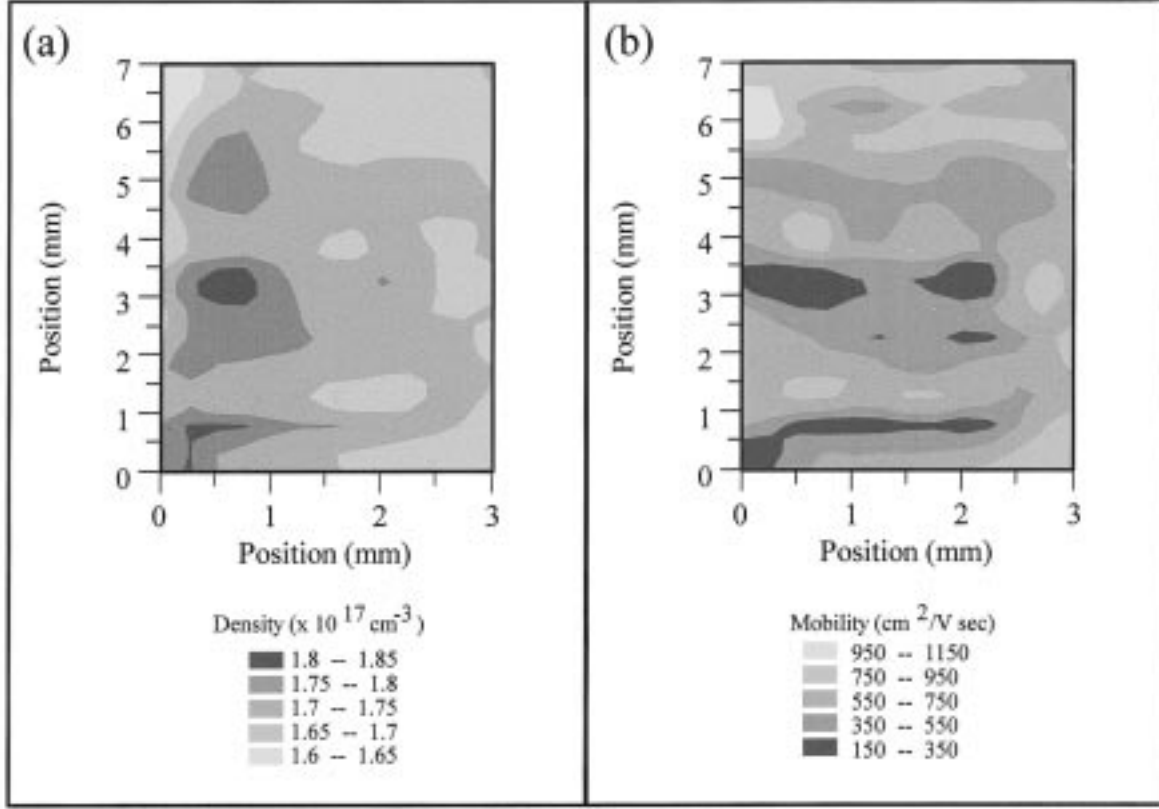


Fig. 15. Terahertz images of the sample from Fig. 14, generated as described in the text. Variations in the doping density are shown in (a), while (b) shows inhomogeneities in the carrier mobility. In each case, the legends show the relation between the color scale and the calculated parameter values.

classification scheme for the recognition of spoken words. Along the same vein, we will in the following discuss some recent approaches in real-time waveform analysis based on signal compression.

The application of digital signal processing techniques [41] in linear spectroscopy involves the modeling of the sample response by linear time-invariant digital filters. In this approach the characteristics of the sample's response is transferred to the digital filter. The most general linear filter takes an input waveform,  $x(t)$ , and produces an output waveform,  $y(t)$ , by the formula

$$y(t) = \sum_{j=0}^N b_j x(t - j\Delta) + \sum_{k=0}^M a_k y(t - k\Delta) \quad (3)$$

where  $a_k$  and  $b_j$  are constant filter coefficients, and  $\Delta$  is the sampling interval. To get some physical insight of the filtering processes we derive the frequency response of the transfer function,  $H(z)$ , corresponding to the time-domain filter described by (3)

$$H(z) = \frac{\sum_{j=0}^N b_j z^{-j}}{1 - \sum_{k=1}^M a_k z^{-k}} \quad (4)$$

where  $z = \exp\{i2\pi f\Delta\}$ , and  $f$  is the frequency. The numerator represents a finite impulse response filter (FIR), and describes a polynomial filtering in  $z^{-1}$ , and hence contains the zeros of the filter. The denominator corresponds to an infinite impulse response filtering (IIR), and describes the poles of the

filter. In order to reduce the complexity of an analysis we will often restrict to use either a pure FIR ( $a_k = 0$ ) or a pure IIR filter ( $b_j = 0$ ) depending on the characteristic response exhibited by the sample. In case of sharp resonances, the IIR filter has proven useful [25], whereas samples that exhibit a smooth frequency response is more appropriately modeled by the FIR filter.

The optimum values of the filter coefficients can be determined directly from the time-domain signal using a correlation type of analysis. The time-domain analysis is based on *least-square* principles. In this approach, one must minimize the squared sum of the difference between the measured signal and the signal generated from the filtering process. The analysis yields a system of linear equations [41] that relates the filter coefficients to values of the cross- and autocorrelation of the sampled waveforms. The system of equations can be solved using matrix inversion. For the pure FIR filtering this type of analysis resembles the memory function analysis that has been recently introduced to THz-TDS [42], [43]. In case of pure IIR filtering, the analysis involves only the autocorrelation of the measured signal, and consequently all phase information is lost. Hence, the IIR filter is only capable of estimating the power absorption spectrum. The use of a pure IIR filtering for parameterization of a digital signal is often referred to as *linear predictive coding* [44].

The IIR filter is efficient for predicting sharp spectral features, which makes it particularly well suited for the analysis of THz-TDS waveforms which have interacted with polar gases.

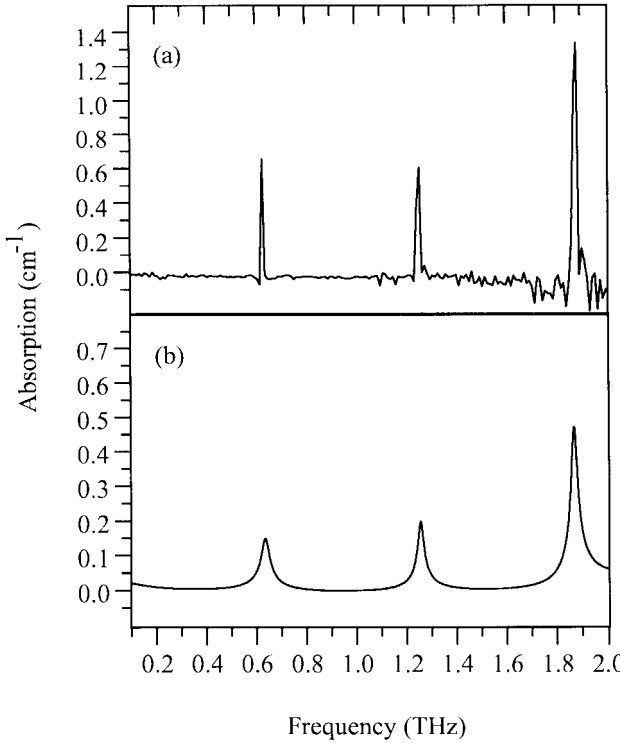


Fig. 16. Absorption spectrum of HCl gas derived by using Fourier analysis (a) or by estimating the power of the IIR filter (b). In (a), 182 of the 1024 Fourier coefficients are displayed. Notice the vertical axes are slightly different. The frequency resolution in the Fourier analysis is better than in the IIR analysis. However, the total power, i.e., the integrated absorption, is the same for the two figures.

The interaction between a broad-band terahertz pulse and a gas consists in a multiple excitation of several resonances. These resonances give rise to a coherent irradiance that follows the impulse excitation [10]. By using an IIR filter approach, one can analyze the characteristic oscillations and perform a classification using simple pattern recognition schemes based on the estimated filter coefficients. As an example, Fig. 16 shows the absorption spectrum of HCl gas at a pressure of 97 torr, with a path length of 30.5 cm. The spectrum is obtained by sampling a waveform of  $N = 1024$  data points, and by using either a conventional Fourier analysis [Fig. 16(a)] or an IIR filter analysis with  $M = 16$  poles [Fig. 16(b)]. For the IIR filter approach, the power spectrum of the sample is estimated from the power spectrum of the filter  $|H(z)|^2$ . The IIR analysis correctly locates the excited resonances, and provides an excellent data compression. The algorithms chosen for the analysis are fast and suitable for real-time chemical recognition. This type of analysis can have technological importance for trace gas monitoring and in quality control.

#### G. Wavelet Analysis

A new and promising mathematical tool known as wavelet transforms has recently entered areas of digital signal processing [45], [46]. Wavelet analysis has been widely used for image compression. In general, the wavelet transform offers high compressibility, and the transform is usually faster than a fast Fourier transform algorithm. In particular, the wavelet

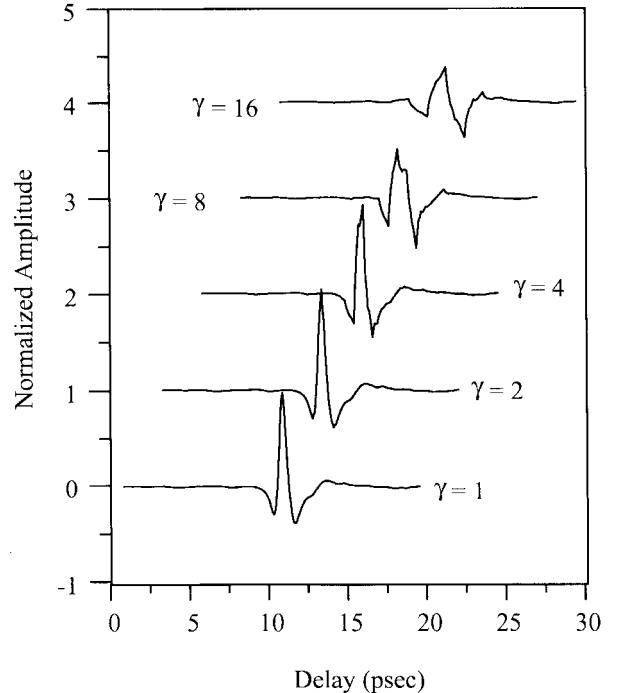


Fig. 17. Waveforms reconstructed from a wavelet transform, truncation, and subsequent inverse wavelet transform, as described in the text. The waveforms have been shifted 2.5 ps in time and 1 unit along the vertical scale for clarity.

transform has proven useful for multiresolution analysis, where one wants to look at a signal at various levels of detail.

A wavelet transform is a decomposition of a signal into a set of basis functions called wavelets. In the time-domain, wavelets are just like ordinary waves that oscillates and decay, and are localized in both time and frequency. In a mathematical sense, the wavelet transform is the correlation between a signal and a *daughter wavelet*. The daughter wavelets,  $h(\frac{t-\tau}{s})$ , are generated from a *mother wavelet*,  $h(t)$ , by dilation,  $s$ , and translation,  $\tau$ . Wavelets are required to satisfy the important criteria of admissibility and regularity [45], [46]. The admissibility criterion states that a waveform must have a zero-mean value. Regularity assures that the first low-order moments vanish. To a large extent the terahertz waveform has these properties. This is supported by the fact that the terahertz waveform does not contain any dc component, and that its spectrum vanishes above a certain frequency. Because of these striking similarities, a wavelet analysis should prove valuable in terahertz waveform analysis.

The first approach to wavelet analysis is a test of the compressibility properties of the wavelet transform. A sampled replica of a terahertz waveform is transformed and subsequently compressed by truncating information at a certain detail level. From the compressed signal we reconstruct the waveform using the inverse wavelet transform (see Fig. 17). The various waveforms in the figure correspond to different compression ratios  $\gamma$ . In the analysis, a basis of orthonormal wavelets known as Daubechies wavelets [45], [46] has been used, and the wavelet transform is performed using a tree pyramidal algorithm. The wavelet filter used consists of only four coefficients, which accounts for the irregular shape of

the reconstructed waveforms. When the length of the filter increases the wavelets become more smooth and regular, at the expense of computational cost.

A wavelet analysis of the type outlined here may prove extremely valuable as a processing algorithm for tomographic data, where the signals may consist of a number of replicas of the input waveform, each modified according to changes in time delay, amplitude, and broadening. In such a case, rapidly extracting these parameters for each replica may be the most important step in the signal processing. In addition, for chemical recognition of materials that have broad spectral features, e.g., liquids and solids, a wavelet multiresolution analysis may be a fast and efficient technique to distinguish between different materials.

## V. OUTLOOK

The previous examples have demonstrated some of the capabilities of the T-ray imaging technology and illustrated its potential for commercial applications. The pulsed nature of the T-ray system and the associated time-domain processing capabilities offer numerous advantages for scientific and commercial applications where information about position, density, or composition is desired. Also, the ability to analyze both amplitude and phase distortions allows one to identify chemical composition in the gas phase, and to a lesser degree also in the liquid and solid phase. T-Ray imaging and other ultrafast optoelectronic technologies are increasingly becoming practical and commercially feasible with the arrival of compact, wall-plug-efficient, and cost-effective femtosecond laser sources. Femtosecond fiber lasers that may find large markets in telecommunications applications will likely bring the size and cost of femtosecond lasers down even further. There are also obvious improvements to the technology that can be pursued. Scanning the T-ray beams instead of the sample is obviously desirable, and a focal-plane T-ray detector array would eliminate the need for scanning altogether, if the application so requires. It is quite clear that the signal processing portion of the T-ray imaging system can be further improved, so that it is faster and more effective in extracting compositional information about the object under investigation.

## VI. CONCLUSION

We have shown how terahertz time-domain spectroscopy can be improved so that it can be extended toward real-time imaging in the terahertz frequency region. This novel "T-Ray" imaging technique, when combined with signal processing and recognition, allows chemically specific imaging of materials, with many potential commercial applications. New techniques like the terahertz Hall effect and T-ray tomography are likely to broaden this applications base, leading to a bright outlook for commercialization of this new and exciting technology.

## ACKNOWLEDGMENT

The authors would like to thank I. Brener and J. Cunningham of Bell Laboratories, Lucent Technologies, M. Geva of Lucent Technologies Microelectronics, B. McMichael and D.

Upchurch of the Agricultural Research Service of the USDA, and M. Brown of Florida State University for important contributions to this project.

## REFERENCES

- [1] P. R. Smith, D. H. Auston, and M. C. Nuss, "Subpicosecond photoconducting dipole antennas," *IEEE J. Quantum Electron.*, vol. 24, pp. 255–260, 1988.
- [2] M. van Exter and D. Grischkowsky, "Characterization of an optoelectronic terahertz beam system," *IEEE Trans. Microwave Theory Tech.*, vol. 38, pp. 1684–1691, 1990.
- [3] M. C. Nuss and J. Orenstein, "Terahertz time-domain spectroscopy (THz-TDS)," in *Millimeter-Wave Spectroscopy of Solids*, G. Gruener, Ed. Heidelberg, Germany: Springer-Verlag, 1997, and references therein.
- [4] B. B. Hu and M. C. Nuss, "Imaging with terahertz waves," *Opt. Lett.*, vol. 20, pp. 1716–1718, 1995.
- [5] Q. Wu, T. D. Hewitt, and X.-C. Zhang, "2-dimensional electro-optic imaging of THz beams," *Appl. Phys. Lett.*, vol. 69, pp. 1026–1028, 1996.
- [6] M. C. Nuss, "Chemistry is right for T-ray imaging," *IEEE Circuits Devices*, vol. 12, pp. 25–30, 1996.
- [7] D. Grischkowsky, S. Keiding, M. van Exter, and C. Fattinger, "Far-infrared time-domain spectroscopy with terahertz beams of dielectrics and semiconductors," *J. Opt. Soc. Amer. B*, vol. 7, pp. 2006–2015, 1990.
- [8] L. Thrane, R. H. Jacobsen, P. Uhd Jepsen, and S. R. Keiding, "THz reflection spectroscopy of liquid water," *Chem. Phys. Lett.*, vol. 240, pp. 330–333, 1995.
- [9] J. T. Kindt and C. A. Schmuttenmaer, "Far-infrared dielectric properties of polar liquids probed by femtosecond terahertz pulse spectroscopy," *J. Phys. Chem.*, vol. 100, pp. 10373–10379, 1996.
- [10] M. van Exter, C. Fattinger, and D. Grischkowsky, "Terahertz time-domain spectroscopy of water vapor," *Opt. Lett.*, vol. 14, pp. 1128–1130, 1989.
- [11] H. Harde, N. Katzenellenbogen, and D. Grischkowsky, "Line-shape transition of collision broadened lines," *Phys. Rev. Lett.*, vol. 74, pp. 1307–1310, 1995.
- [12] L. Rabiner and B.-H. Juang, *Fundamentals of Speech Recognition*, A. V. Oppenheim, Ed. Englewood Cliffs, NJ: Prentice Hall, 1993.
- [13] N. H. Rizvi, P. M. W. French, and J. R. Taylor, "50-fs pulse generation from a self-starting CW passively mode-locked Cr:LiSrAlF<sub>6</sub> laser," *Opt. Lett.*, vol. 17, pp. 877–879, 1992.
- [14] D. Kopf, K. J. Weingarten, L. R. Brovelli, M. Kamp, and U. Keller, "Diode-pumped 100-fs passively mode-locked Cr:LiSAF laser with an antiresonant Fabry-Perot saturable absorber," *Opt. Lett.*, vol. 19, pp. 2143–2145, 1994.
- [15] S. Tsuda, W. H. Knox, E. A. De Souza, W. Y. Jan, and J. E. Cunningham, "Low-loss intracavity AlAs/AlGaAs saturable Bragg reflector for femtosecond mode locking in solid-state lasers," *Opt. Lett.*, vol. 20, pp. 1407–1409, 1995.
- [16] S. Tsuda, W. H. Knox, and S. T. Cundiff, "High efficiency diode pumping of a saturable Bragg reflector-mode-locked Cr:LiSAF femtosecond laser," *Appl. Phys. Lett.*, vol. 69, pp. 1538–1540, 1996.
- [17] I. Brener, D. Dykaar, A. Frommer, L. N. Pfeiffer, J. Lopata, J. Wynn, K. West, and M. C. Nuss, "Terahertz emission from electric field singularities in biased semiconductors," *Opt. Lett.*, vol. 21, pp. 1924–1926, 1996.
- [18] D. Krökel, D. Grischkowsky, and M. B. Ketchen, "Subpicosecond electrical pulse generation using photoconductive switches with long carrier lifetimes," *Appl. Phys. Lett.*, vol. 54, pp. 1046–1048, 1989.
- [19] N. Katzenellenbogen and D. Grischkowsky, "Efficient generation of 380 fs pulses of THz radiation by ultrafast laser pulse excitation of a biased metal-semiconductor interface," *Appl. Phys. Lett.*, vol. 58, pp. 222–224, 1991.
- [20] S. Gupta, M. Y. Frankel, J. A. Valdmanis, J. F. Whitaker, G. A. Mourou, F. W. Smith, and A. R. Calawa, "Subpicosecond carrier lifetime in GaAs grown by molecular beam epitaxy at low temperatures," *Appl. Phys. Lett.*, vol. 59, pp. 3276–3278, 1991.
- [21] P. Uhd Jepsen and S. R. Keiding, "Radiation patterns from lens-coupled terahertz antennas," *Opt. Lett.*, vol. 20, pp. 807–809, 1995.
- [22] R. A. Cheville and D. Grischkowsky, "Time domain terahertz impulse ranging studies," *Appl. Phys. Lett.*, vol. 67, pp. 1960–1962, 1995.
- [23] F. A. Jenkins and H. E. White, *Fundamentals of Optics*, 4th ed. New York: McGraw Hill, 1976, pp. 166–167.
- [24] M. C. Nuss, U. Keller, G. T. Harvey, M. S. Heutmaker, and P. R. Smith, "Amplitude noise reduction of 50 dB in colliding pulse mode-locking dye lasers," *Opt. Lett.*, vol. 15, pp. 126–128, 1990.

- [25] R. H. Jacobsen, D. M. Mittleman, and M. C. Nuss, "Chemical recognition of gases and gas mixtures using terahertz waveforms," *Opt. Lett.*, vol. 21, pp. 2011–2013, 1996.
- [26] J. D. Jackson, *Classical Electrodynamics*, 2nd ed. New York: Wiley, 1975, pp. 422–423.
- [27] N. C. Turner, R. A. Spurway, and E. D. Schulze, "Comparison of water potentials measured by *in situ* psychrometry and pressure chamber in morphologically different species," *Plant Physiol.*, vol. 74, pp. 316–319, 1984.
- [28] R. A. Cheville and D. Grischkowsky, "Far-infrared terahertz time-domain spectroscopy of flames," *Opt. Lett.*, vol. 20, pp. 1646–1648, 1995.
- [29] J. C. Owens, "Optical refractive index of air: Dependence on pressure, temperature and composition," *Appl. Opt.*, vol. 6, pp. 51–59, 1967.
- [30] D. M. Mittleman and M. C. Nuss, "T-ray tomography," *Opt. Lett.*, submitted for publication.
- [31] D. Huang, E. A. Swanson, C. P. Lin, J. S. Schuman, W. G. Stinson, W. Chang, M. R. Hee, T. Flotte, K. Gregory, C. A. Puliafito, and J. G. Fujimoto, *Science*, vol. 254, pp. 1178–1181, 1991.
- [32] G. J. Tearney, M. E. Brezinski, J. F. Southern, B. E. Bouma, M. R. Hee, and J. G. Fujimoto, *Opt. Lett.*, vol. 20, pp. 2258–2260, 1995.
- [33] Z. B. Niazi, T. J. Essex, R. Papini, D. Scott, N. R. McLean, and M. J. Black, "New laser doppler scanner, a valuable adjunct in burn depth assessment," *Burns*, vol. 19, pp. 485–489, 1993.
- [34] L. Atiles, W. Mileski, G. Purdue, J. Hunt, and C. Baxter, "Laser doppler flowmetry in burn wounds," *J. Burn Care Rehabil.*, vol. 16, pp. 388–393, 1995.
- [35] D. M. Mittleman and M. C. Nuss, "The terahertz Hall effect," *Appl. Phys. Lett.*, accepted for publication.
- [36] R. G. Chambers and B. K. Jones, "Measurement of the high-field Hall effect by an inductive method," in *Proc. Roy. Soc. Lon. A*, vol. 270, pp. 417–434, 1962.
- [37] M. Golosovsky and D. Davidov, "Novel millimeter-wave near-field resistivity microscope," *Appl. Phys. Lett.*, vol. 68, pp. 1579–1581, 1996.
- [38] N. Katzenellenbogen and D. Grischkowsky, "Electrical characterization to 4 THz of *N*- and *P*-type GaAs using THz time-domain spectroscopy," *Appl. Phys. Lett.*, vol. 61, pp. 840–842, 1992.
- [39] M. van Exter and D. Grischkowsky, "Carrier dynamics of electrons and holes in moderately doped silicon," *Phys. Rev. B*, vol. 41, pp. 12140–12149, 1990.
- [40] M. C. Nuss, K. W. Goossen, J. P. Gordon, P. M. Mankiewich, M. L. O'Malley, and M. Bhushan, "Terahertz time-domain measurement of the conductivity and superconducting band gap in niobium," *J. Appl. Phys.*, vol. 70, pp. 2238–2241, 1991.
- [41] J. G. Proakis and D. G. Manolakis, *Digital Signal Processing, Principles, Algorithms, and Applications*. Englewood Cliffs, NJ: Prentice Hall, 1996.
- [42] J. E. Pedersen and S. R. Keiding, "THz time-domain spectroscopy of nonpolar liquids," *IEEE J. Quantum Electron.*, vol. 28, pp. 2518–2522, 1992.
- [43] B. Flanders, R. Cheville, D. Grischkowsky, and N. F. Scherer, "Pulsed terahertz spectroscopy of solutions: Experiment and memory function analysis," in *Ultrafast Phenomena X, OSA Tech. Dig. Ser.*, vol. 8. Washington, DC: Opt. Soc. Amer., 1996, pp. 254–255.
- [44] J. Makhoul, "Linear prediction: A tutorial review," *Proc. IEEE*, vol. 63, pp. 561–580, 1975.
- [45] Y. Sheng, "Wavelet transform," in *The Transform and Application Handbook*, A. D. Poularikas, Ed. Piscataway, NJ: IEEE, 1996, pp. 747–827.
- [46] J. Kovacevic and I. Daubechies, Eds., "Special issue on wavelets," *Proc. IEEE*, vol. 84, 1996.



**Daniel M. Mittleman** was born in Berkeley, CA, in 1966. He received the B.S. degree in physics from the Massachusetts Institute of Technology in 1988, and the M.S. and Ph.D. from the University of California, Berkeley, in 1990 and 1994, respectively, both in physics.

He spent two years as a Post-Doctoral Member of the Technical Staff at AT&T Bell Laboratories (now Bell Laboratories—Lucent Technologies). He is now a Faculty Fellow in the Electrical and Computer Engineering Department at Rice University.

His research interests include both spectroscopy and applications of terahertz time-domain spectroscopy.

Dr. Mittleman is a member of the Optical Society of America and the American Physical Society.



**Rune H. Jacobsen** was born in Copenhagen, Denmark, on October 12, 1970. He received the B.Sc. degree in physics from Odense University, Denmark, in 1992, the M.Sc. degree in chemistry from Aarhus University, Denmark, in 1995, and is currently pursuing the Ph.D. degree.

In 1996, he conducted part of his graduate research program as a visiting scientist with the Advanced Photonics Research Department at Bell Laboratories, Lucent Technologies, USA. His principal research interests include the generation and detection terahertz bandwidth electromagnetic pulses for ultrafast spectroscopic purposes and for the characterization of high-speed electronics.



**Martin C. Nuss** (M'90) was born in Lörrach, Germany, in 1957. In 1982, he received the Diploma and in 1985 the Dr. Rer. Nat. degree in physics, both from the Technical University Munich, Germany.

He joined Bell Laboratories in 1985 as a post-doctoral member in Murray Hill, NJ, and has been a Member of Technical Staff in Holmdel, NJ, since 1987. His work in ultrafast optoelectronics led to the use of terahertz bandwidth electromagnetic transients for time-resolved spectroscopy at far-infrared frequencies. He has studied phonon polaritons in electro-optic materials, hot carriers in semiconductors, dissipation processes in superconductors, and intersubband transitions in semiconductor nanostructures. He also demonstrated charge oscillations in semiconductor quantum wells, and was the first to show coherent control of these oscillations. More recently, he brought terahertz spectroscopy to the commercial arena through the invention of T-ray imaging, and is working on communications applications of femtosecond technology, notably for wavelength-division-multiplexing.

Dr. Nuss is a member of the Optical Society of America, the American Physical Society, and the IEEE Lasers and Electro-Optics Society.